IMPROVED RESOLUTION LUNAR PROSPECTOR NEUTRON AND GAMMA-RAY DATA. J. T. Wilson[1,*] D. J. Lawrence[1], P. N. Peplowski[1], V. R. Eke[2], R. J. Massey[2] and L. F. A. Teodoro[3]. [1]The Johns Hopkins University Applied Physics Laboratory, 11100 Johns Hopkins Road, Laurel, MD 20723, USA, [2]Institute for Computational Cosmology, Department of Physics, Durham University, Science Laboratories, South Road, Durham, DH1 3LE, UK. [3] BAERI/NASA Ames, Moffat Field, CA 94035, USA. [*]Jack.Wilson@jhuapl.edu.

Introduction: The global distribution of all major and several minor elements on the Moon was mapped by the Lunar Prospector (LP) Gamma-Ray (GRS) and Neutron Spectrometers (NS) [e.g. 1,2,3]. Information in these maps has given rise to an improved understanding of the formation and evolution of the lunar surface and interior [e.g. 4]. Unlike other spectroscopic techniques, both gamma-ray and neutron spectroscopy have the advantage of being able to provide bulk measurements of elemental composition at depths of a few tens of cm, which is orders of magnitude deeper than that available from ultraviolet to near-infrared spectroscopy.

Planetary neutron data are typically separated into three energy ranges: high-energy, fast neutrons (500 keV < E 10 < MeV); intermediate energy, epithermal neutrons (0.3 eV < E < 500 keV) and slower, thermal neutrons (E < 0.3 eV). Epithermal neutron data are sensitive to the presence of hydrogen and the LP-NS epithermal data have revealed the presence of subsurface hydrogen at the poles [5,6], which is preferentially concentrated within the cold traps within permanently shaded regions [6,7]. Thermal neutron data provide a map of neutron absorbing elements, which on the Moon are predominately Fe, Ti and rare earth elements (REE) [8]. Analysis of these data to create maps of absolute neutron absorption also revealed the presence of nearly pure plagioclase in parts of the highlands [9]. The fast neutron data provide the most robust measurement of mean atomic mass within the top metre of lunar regolith.

In addition to their ability to measure bulk elemental abundance, the penetrating power of gamma rays and neutrons leads to the spatial response functions of orbital GRS and NS being similar to the spacecraft's altitude. Thus spatial resolution is improved by lowering orbital altitude. This relatively large point spread function (PSF) hinders comparison with other, better-resolution, remotely-sensed data, such as visible imaging, due to the blurring effects of observation with the GRS/NS. This averaging also results in a reduction of the dynamic range of the measured data.

An efficient method of reducing these complications with GRS/NS data is the application of image reconstruction techniques to sharpen the maps and suppress the effects of noise. We have applied the Pixon image reconstruction technique [10,11,12] to the LPNS and Th line GRS data to improve their resolution and suppress noise present in the data.

Image reconstruction in planetary sciences: Observation by an imperfect instrument can often be modelled by stating that the data obtained, D, are the result of the convolution of the true, underlying, image, I, that would be measured with a perfect instrument, with the PSF of the actual detector, B, and the addition of noise, N, i.e.

$$D(\mathrm{x}) = I * B(\mathrm{x}) + N(\mathrm{x}). \qquad (1)$$

where the argument x refers to position or pixel number (as appropriate) and $*$ is the spatial convolution operator. Solving for the inverse of equation (1) to find the reconstruction closest to the original image, I, is the problem of image reconstruction. As the noise is

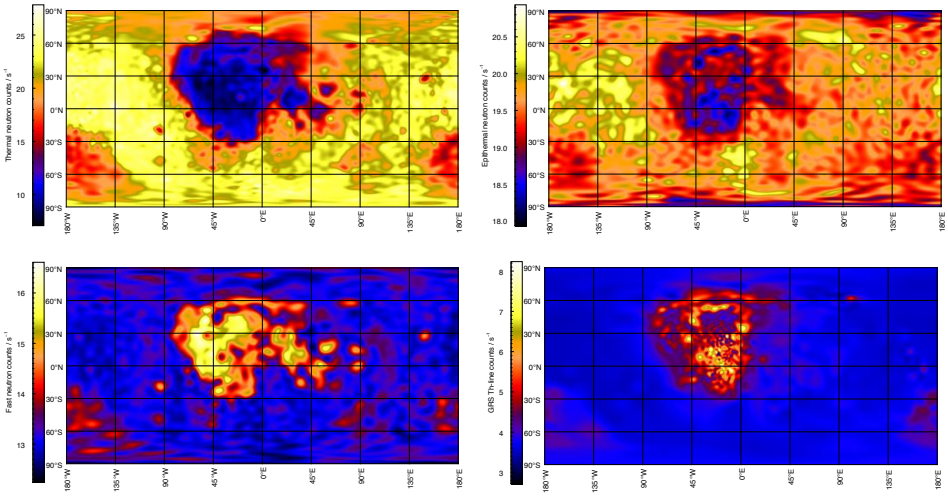

Figure 1: *Clockwise from top left*: Maximum entropy pixon reconstruction of the Lunar Prospector thermal, epithermal and fast neutron data and Locally adaptive pixon reconstruction of the Lunar Prospector GRS Th-line data.

known only statistically, equation (1) cannot be inverted analytically so we must instead adopt some statistical or iterative technique to perform the inversion.

Bayesian image reconstruction techniques have been developed that make use of prior information, favouring simplicity, in addition to the measured data. The Bayesian technique most often employed in the reconstruction of planetary neutron and gamma ray data is the pixon method [10,11,12].

It was noted by Pina and Puetter [10] that each cell, or pixel, represents a degree of freedom and in regions of the image with low signal to noise ratio or containing little structure this may cause the image to be over specified. Grouping sets of pixels together would remove this problem and greatly improve the prior, which is strongly dependent on the number of cells. It is these groups of pixels, called pixons, that form the fundamental image units in pixon reconstructions.

The pixon method has recently been used to reconstruct remotely sensed neutron [7,12] and gamma ray data [14, 15] and has been shown to give a spatial resolution 1.5-2 times that of other methods in reconstructing planetary data sets [14].

Results: The results of the global pixon reconstructions of each of the LP data sets are shown in Figure 1. Maximum entropy pixon reconstructions of the neutron data are shown as is a locally adaptive pixon reconstruction of the LPGRS Th-line data. Several surface features are brought into sharper detail in the reconstructions one of which is described below.

Schrodinger basin. The Schrodinger basin, located at 75°S, 135°E has a diameter of ~ 320 km with a peak ring of diameter ~ 150 km. On the basis of spectral data this peak ring has been confirmed as containing km-scale regions of pure or nearly pure anorthosite [16]. Additionally, the basin contains a large pyroclastic deposit, visible as a darker region in the left panel of Figure 2 at 75°S, 140°E, with the vent from which the deposit was sourced observable in the shaded relief in the right hand panel.

The effect of performing a pixon reconstruction on the data is seen by comparing the panels in Figure 8. Before reconstruction the separate features in the basin cannot be resolved, after reconstruction the pyroclastic deposit and western limb of the peak ring are clearly seen. The absence of a clear eastern limb in the thermal neutron data is either the result of its proximity to the pyroclastic deposit and the resolution limitations of even the reconstructed data or an indication that the western limb is more plagioclase rich. Indeed, there are a greater number of spectral detections of pure anorthosite in the west of the peak rim [16]. However at such polar latitudes the angle of solar incidence places constraints on the completeness of spectral data.

References: [1] Elphic, R. C. et al. (1998) Science, 281, 1493. [2] Feldman, W. C. et al. (1998) Science, 281, 1489. [3] Lawrence, D. J. et al (1998) Science, 281, 1484. [4] Jolliff, B. J. et al. (2000) JGR, 105, 4197–4216. [5] Feldman W. C. et al. (2000) JGR, 105, 20347–20364. [6] Feldman W. C. et al. (2001) JGR, 106, 23231– 23252. [7] Eke, V. R. et al. (2009) Icarus, 200, 12–18. [8] Elphic, R. C. et al. (2000) JGR, 105, 20333–20346. [9] Peplowski, P. N. et al. (2016) JGR, 121, 388–401 [10] Pina, R. K. and Puetter, R. C. (1993), PASP, 105, 630–637. [11] Eke, V. (2001) MNRAS, 324, 108–118. [12] Wilson, J. T. et al. (2018) Icarus, 299, 148–160 [14] Lawrence, D. J. et al. (2007) GRL, 34, 3201. [15] Wilson, J. T. et al. (2015) JGR, 120, 92–108. [16] Kramer, G. Y. (2013) Icarus, 223, 131–148.

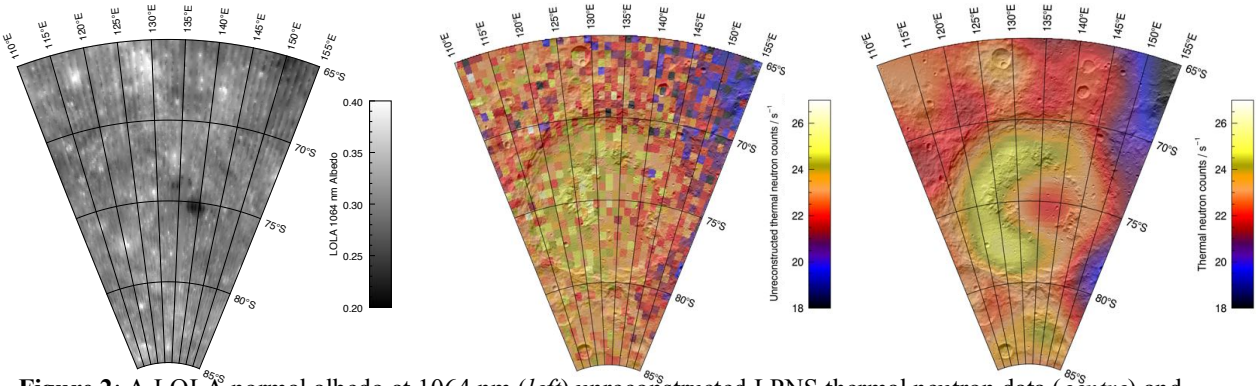

Figure 2: A LOLA normal albedo at 1064 nm (*left*) unreconstructed LPNS thermal neutron data (*centre*) and maximum entropy pixon (*right*) reconstruction of the Lunar Prospector thermal neutron data at Schro¨dinger crater. The neutron data are superimposed on a LOLA shaded relied image.